

Proliferation of unstable states and their impact on stochastic out-of-equilibrium dynamics in two coupled Kerr parametric oscillators

Toni L. Heugel,¹ R. Chitra,¹ Alexander Eichler^{2,3} and Oded Zilberberg⁴

¹*Institute for Theoretical Physics, ETH Zurich, CH-8093 Zurich, Switzerland*

²*Laboratory for Solid State Physics, ETH Zurich, CH-8093 Zurich, Switzerland*

³*Quantum Center, ETH Zurich, CH-8093 Zurich, Switzerland*

⁴*Department of Physics, University of Konstanz, D-78457 Konstanz, Germany*



(Received 14 July 2023; revised 6 February 2024; accepted 31 May 2024; published 20 June 2024)

Networks of nonlinear parametric resonators are promising candidates as Ising machines for annealing and optimization. These many-body out-of-equilibrium systems host complex phase diagrams of coexisting stationary states. The plethora of states manifest via a series of bifurcations, including bifurcations that proliferate purely unstable solutions. Here we demonstrate that the latter take a fundamental role in the stochastic dynamics of the system. Specifically, they determine the switching paths and the switching rates between stable solutions. We demonstrate experimentally the impact of the added unstable states on noise-activated switching dynamics in a network of two coupled parametric resonators.

DOI: [10.1103/PhysRevE.109.064308](https://doi.org/10.1103/PhysRevE.109.064308)

I. INTRODUCTION

Statistical physics has provided valuable insights into the phenomenon of noise-induced switching between local energy minima, as exemplified by the well-known Kramers double-well problem [1–3]. Such stochastic dynamics is highly relevant for a wide variety of phenomena spanning protein folding [4,5] and chemical reactions [6], as well as stability in mechanical [3,7] and electrical systems [8,9]. While the noisy dynamics of equilibrium systems have been extensively studied, that of systems driven far out of equilibrium remains largely unexplored [10–12].

An important class of out-of-equilibrium systems are driven systems. Such systems are characterized by stationary oscillation states that manifest when the conserving and non-conserving forces in the system are in balance. For nonlinear systems, there may be several such stationary states that act as attractors, just like potential wells do in equilibrium systems. In a rotating frame, the resulting dynamics can resemble that of an equilibrium potential landscape [2]. Extending the analogy, weak noise can induce stochastic switching between the attractors, and the switching rate can be treated with the abstract notion of a potential activation barrier [10,13–21]. However, it is important to emphasize that this activation barrier is not related to a gap in free energy, but instead to a “phase gap” that separates the attractors [22]. Understanding how often the system switches between attractors, and which path it selects during the switch, requires different methods and can be cumbersome [2,10].

A paradigmatic example of a bistable out-of-equilibrium system is the Kerr parametric oscillator (KPO) [22–37]. The KPO is a resonator whose potential term is periodically modulated (“pumped”) at a rate close to twice its natural frequency. This modulation can exponentially amplify oscillations, such that the system enters a state whose amplitude is determined by the Kerr nonlinearity. Since the pumping occurs at twice

the resonance frequency, there are two such states with opposite phases. Recently, networks of coupled, driven KPOs have been proposed as a simulation platform to solve complex problems optimally [38–45]. Such networks typically possess a large number of stationary states, analogous to a multiwell potential with rich phase transitions [46–49]. Studying activated switching between states in the presence of fluctuations is crucial for understanding their stability and lifetimes. It will influence how these networks are operated, and it can also provide a characterization method that is unaffected by the danger of local trapping [50].

In this work we address the physics of stochastic activation in a tractable system of two strongly coupled, classical KPOs. The system possesses various stable and unstable stationary states [48,51], and we observe stochastic switching between two stable states in the presence of fluctuations. Surprisingly, the switching rate Γ deviates significantly from the exponential model expected for a single KPO [10]. Seeking to explain this deviation, we calculate the dominant transition paths between the states with the Onsager-Machlup function [52,53]. Our analysis shows that several unstable states emerge in the two-KPO system. These states do not manifest in the stationary deterministic dynamics of the system. Interestingly, however, they offer new transition paths and contribute significantly to the corresponding transition rates. We thus identify a striking example of out-of-equilibrium statistical physics in a nonlinear multistable system. Our work paves the way for the exploration of larger systems, especially in view of KPO networks as solvers for complex optimization tasks.

II. SYSTEM

In the following we analyze noise-induced switching dynamics using an experimental setup composed of two electrical KPOs with capacitive coupling [32,48]. Each KPO

consists of a coil with inductance L and a diode that provides a nonlinear capacitance C ; cf. Appendix A. The resonance frequency of each KPO can be tuned by applying a DC voltage across the diode. We drive and measure the resonators inductively through auxiliary coils. Our electrical circuits are well described by the following coupled equations of motion:

$$\ddot{x}_i + \omega_i^2 [1 - \lambda \cos(2\omega_d t)] x_i + \alpha_i x_i^3 + \gamma_i \dot{x}_i - \sum_{j \neq i} J_{ij} x_j = \xi_i(t), \quad (1)$$

where dots indicate time derivatives, $x_i = u_i \cos(\omega t) - v_i \sin(\omega t)$ is the measured voltage with quadrature amplitudes u_i and v_i , $\omega_i = 2\pi f_i$ is the angular eigenfrequency, and J_{ij} ($i \neq j$) denotes the intercircuit linear coupling strength. Each resonator has an effective Duffing (Kerr) nonlinearity with coefficient α_i and a damping rate $\gamma_i = \omega_i/Q_i$, with Q_i the quality factor. Our resonators are constructed and tuned to be (nearly) identical in their bare characteristics, $\omega_i \approx \omega_0 = 2\pi f_0$. The same parametric pumping with angular modulation frequency $2\omega_d = 4\pi f_d \approx 2\omega_0$ and modulation depth $\lambda \propto U_d$ is applied to all resonators.

Crucially, beyond a frequency-dependent driving threshold U_{th} , the KPO has exactly two stable solutions that we refer to as “phase states,” which have identical amplitudes but differ in phase by π [37,54,55]. These are the two attractors of a single KPO in a frame rotating at ω_d . In order to induce switching events between the attractors, we add an artificial noise ξ_i generated by a fluctuating voltage with white power spectral density S_n . The noise ξ_i simulates a thermal force noise with $\langle \xi_i(t_1) \xi_j(t_2) \rangle = \zeta^2 \delta_{ij} \delta(t_1 - t_2)$ and power spectral density calibrated to be $\zeta^2 = 4.93 \times 10^{-20} \text{ Hz}^4 S_n$; see Appendix B. Note that the applied noise lies within the so-called weak noise limit, except in the immediate vicinity of bifurcation points in our system [56–60].

In our experiments, we use a lock-in amplifier to measure the quadratures (u_i, v_i), which vary on timescales much longer than $1/\omega_0$. The evolution of these quadratures is well captured in the rotating-frame picture obtained by applying the averaging method [51,61–63] to our model. Equation (1) then leads to the following slow-flow equations:

$$\begin{aligned} \dot{u}_i &= -\frac{\gamma u_i}{2} - \left(\frac{3\alpha}{8\omega_d} X_i^2 + \frac{\omega_0^2 - \omega_d^2}{2\omega_d} + \frac{\lambda\omega_0^2}{4\omega_d} \right) v_i + \frac{Jv_j}{2\omega_d} + \Xi_{u_i}, \\ \dot{v}_i &= -\frac{\gamma v_i}{2} + \left(\frac{3\alpha}{8\omega_d} X_i^2 + \frac{\omega_0^2 - \omega_d^2}{2\omega_d} - \frac{\lambda\omega_0^2}{4\omega_d} \right) u_i - \frac{Ju_j}{2\omega_d} + \Xi_{v_i}, \end{aligned} \quad (2)$$

with quadratures defined via

$$x_i = X_i \text{Re}[e^{i(\omega_d t + \phi)}] = u_i \cos(\omega_d t) - v_i \sin(\omega_d t), \quad (3)$$

and we can use the trigonometric identity

$$X_i^2 = u_i^2 + v_i^2. \quad (4)$$

The additive uncorrelated noise terms Ξ_{u_i}, Ξ_{v_i} are the cosine and sine components of the noise ξ_i filtered over one oscillation period and have power spectral densities given by $\sigma^2 = \zeta^2/2\omega_d^2$ [64,65]. For more details, please also consult Sec. 4.2.2 of Ref. [37] for the averaging method in the case of a stochastic driving term. As shown in previous works, the

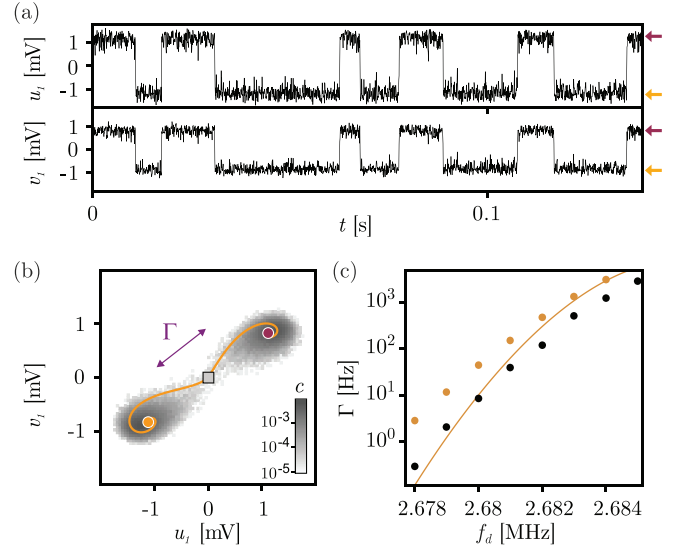


FIG. 1. Noise-induced switching in a single KPO. (a) Time trace of the rotating quadratures u_1 and v_1 , showing noisy fluctuations around and switching between the two phase states for $U_d = 3$ V and $S_n = 2.75 \times 10^{-8} \text{ V}^2 \text{ Hz}^{-1}$ at $f_d = 2.681$ MHz. Arrows indicate the position of the phase states. (b) Heat map of normalized measurement counts c vs u_1 and v_1 , showing two dominant attractors around the phase states (colored dots). The data stem from a time trace measurement as in (a) taken over 8 s. Counts close to the origin arise due to interstate switching with rate Γ . The orange line shows the most probable switching path through the origin (gray square) predicted from the Onsager-Machlup formalism; cf. Eq. (5) and Appendix A. (c) Switching rate Γ as a function of f_d with the same parameters as in (a) obtained from the experiment (black dots) [21]. The orange line corresponds to the approximate analytical result from Ref. [10] (cf. Appendix C) and the orange dots to numerical minimization of Eq. (5).

averaging method fully captures the physics of our networks in the regime where $\lambda, \gamma/\omega_0, J/\omega_0^2, (\alpha/\omega_0^2)x_i^2$, and $\alpha\zeta^2/\omega_0^5$ are all of order ϵ with $0 < \epsilon \ll 1$ [31,62,64,66]. Here and in the following, we assume identical dissipation rates $\gamma_i = \gamma$, nonlinearities $\alpha_i = \alpha$, and coupling $J_{ij} = J$.

III. TRANSITION RATES

A switching experiment with KPO 1 (while KPO 2 is detuned) is shown in Fig. 1(a). We tune the parametric drive amplitude λ and frequency ω_d into the region where only the two phase states are stable [37]. There, due to the added noise, we observe that the system resides in each phase state for a certain dwell time before switching to the opposite state. The average dwell time τ can be expressed as a rate of activated switching $\Gamma = \tau^{-1}$. In the rotating phase space, the same measurement data can be represented as a density of count rates; see Fig. 1(b). As discussed in Ref. [10], the logarithm of the switching rate is inversely proportional to the distance between the two phase states. In Fig. 1(c) this leads to an exponential decrease in Γ with decreasing f_d (the direction in f_f in which Γ increases depends on the sign of the nonlinearity). We measure the switching rate as discussed in Ref. [21].

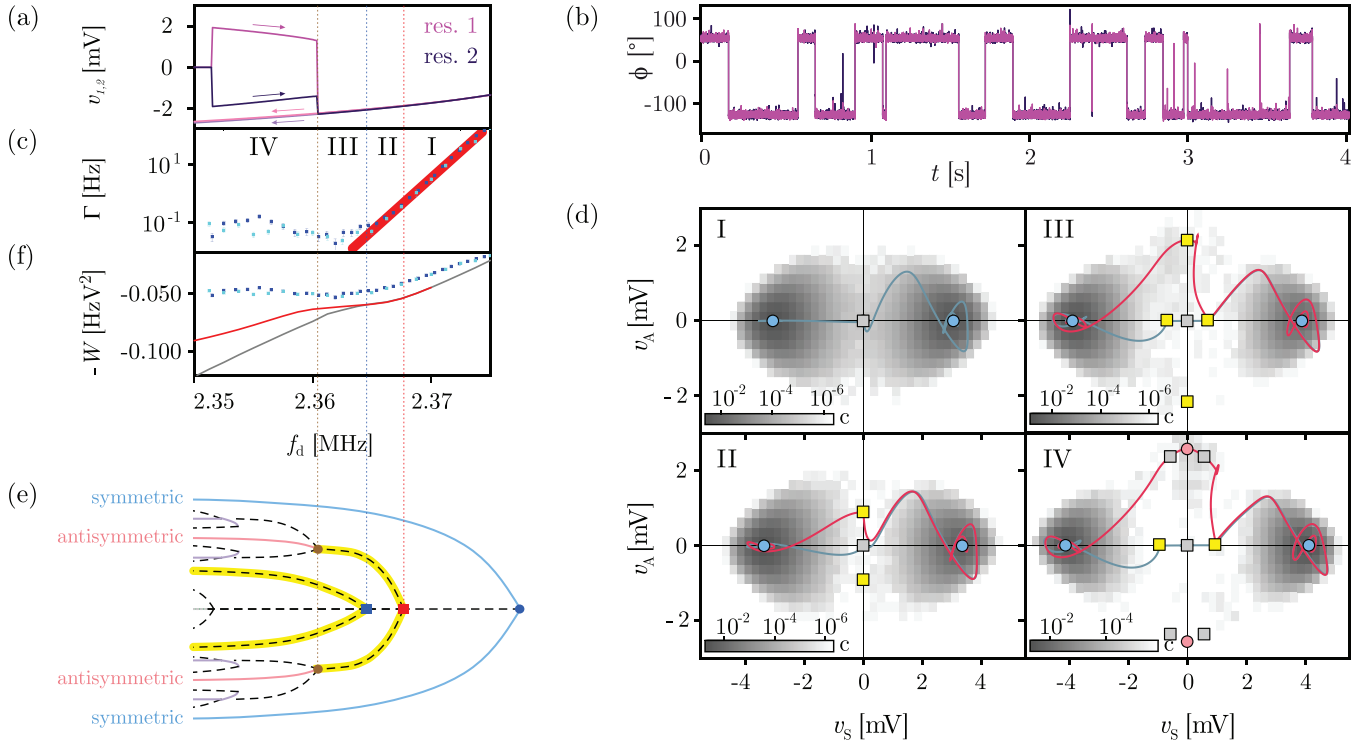


FIG. 2. Noise-induced switching in the two-KPO system. (a) Quasistatic frequency sweep with a parametric drive $U_d = 3.7$ V applied to both resonators. Full data (including the $u_{1,2}$ and the stability diagram) are shown in Fig. 3. Arrows indicate the sweep direction. Vertical dashed lines indicate the bifurcation frequencies; cf. (e). (b) Switching between the two symmetric phase states at $f_d = 2.37$ MHz in the presence of applied voltage noise (see Appendix B for details). (c) Switching rate Γ as a function of f_d for a noise PSD $S_n = 1.1 \times 10^{-7}$ V² Hz⁻¹. Dark (light) blue corresponds to experimental (simulated) data with error bars estimated from textbook Poisson statistics. A thick red line reflects the exponential trend. (d) Switching between the two symmetric states visualized in the rotating frame in terms of v_S and v_A . I: 2.37 MHz, II: 2.3675 MHz, III: 2.3625 MHz, IV: 2.36 MHz. Grayscale heat maps represent the normalized counts c from multiple switches. Circles and squares indicate stable and unstable solutions, respectively. The ghost states are marked in yellow. The solid lines are the theoretically predicted switching paths between the stable symmetric states using the Onsager-Machlup formalism; cf. Eq. (5). The color indicates whether a path passes the unstable ghost state (red) or the unstable zero-amplitude state (blue-gray). (e) Schematics of the steady states and bifurcation points as a function of f_d . Solid and dashed lines are for stable and unstable solutions, respectively. Squares mark ghost bifurcations that proliferate additional unstable states (ghost states) from an already unstable solution. Ghost states are marked in yellow; see Refs. [48,49] for a systematic study of our model's (1) bifurcations and their stability as a function of all tuning parameters. (f) Activation W as a function of f_d . Dark (light) blue corresponds to experimental (simulated) data with error bars estimated from textbook Poisson statistics. The solid gray and red lines are obtained by minimizing S_{OM} for paths via the zero-amplitude state and the antisymmetric state, respectively. The system parameters are: $Q = 265$, $f_0 = 2.3670$ MHz, $\alpha = -6.5 \times 10^{17}$ V⁻²s⁻², $U_{th} = 1.73$ V, and $J = -1.28$ MHz².

We now consider the case that the two KPOs are tuned to have the same frequency. A detailed experimental phase diagram of the system, including a bifurcation (and stability) analysis as a function of λ and ω_p , was explored in Refs. [48,49]. In Fig. 2(a) we show the results of a specific measured frequency sweep passing through various regions containing up to four different types of stable two-oscillator states: a state with both resonators having amplitude zero; symmetric states, i.e., the two oscillators have the same phase; antisymmetric states where the two oscillators have π -shifted phases; and mixed-symmetry states that are neither symmetric nor antisymmetric. The symmetric/antisymmetric solutions can be interpreted as the parametrically driven symmetric/antisymmetric normal modes of the two resonators. See Fig. 3 for more information regarding the stability diagram.

Typically, when initialized in one such state, the resonator explores the vicinity of the attractor under the influence of the

noise terms Ξ_{u_i} and Ξ_{v_i} [49]. Occasionally, the noise activates the system over the quasipotential barrier to reach a different attractor, as seen, for instance, in Fig. 2(b) [21]. The system can switch back and forth in time and is characterized by switching rates Γ_{ij} between any two attractors $i \neq j$. In the following, we analyze the rate Γ of switching between the two symmetric phase states along the sweep in Fig. 2(a). We choose a drive amplitude $\lambda > J$, where for $f_d > 2.36$ MHz, only the symmetric solution is stable [48]. We therefore expect $\Gamma(f_d)$ to manifest an exponential behavior analogous to that seen in a single KPO in Fig. 1. Motivated by this idea, we set out to confirm the hypothesis that each normal mode has the same activation rate scaling as a single KPO.

In Fig. 2(c) we show the measured transition rate Γ for switches between the two symmetric states as a function of f_d while the parametric driving strength U_d is fixed. With decreasing f_d , the transition rate Γ decreases exponentially as expected from previous single KPO studies [10,18,21,23,67].

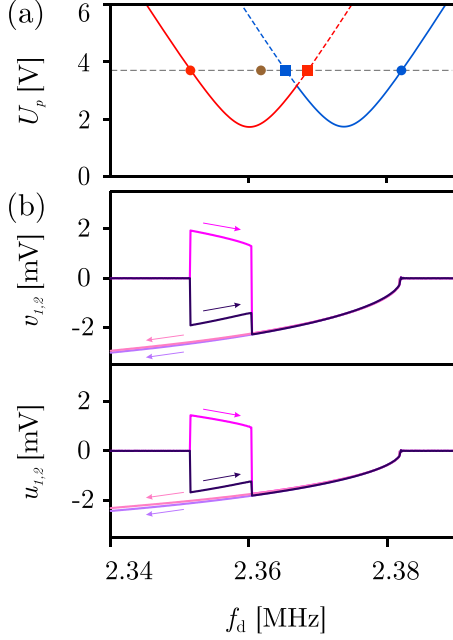


FIG. 3. (a) Stability diagram of the system of two coupled KPOs in a space spanned by f_d and U_p . The red and blue lines mark the instability lobes of the parametrically driven antisymmetric and symmetric normal modes, respectively. The frequency sweep in Fig. 2(a) and in (b) of this figure was taken at the U_p value indicated by a dashed horizontal line, with dots and squares corresponding to the bifurcations shown in Fig. 2(e). (b) Full data of the frequency sweep shown in Fig. 2(a). Arrows indicate the sweep direction.

This holds for a distinct range marked as I and II until $f_d \approx 2.365$ MHz is reached. Surprisingly, below this frequency, we observe substantial deviations from the simple exponential model even though the symmetric state remains the only stable configuration. First, a kink manifests at $f_d = 2.365$ MHz, implying a relative enhancement of the switching in region III. At even lower frequencies, the slope of Γ changes sign, signaling a significant increase of the switching with decreasing frequency in region IV. This behavior is fundamentally at odds with the standard expectation of decreasing rates.

To obtain deeper insights into the curious switching behavior of the two-KPO system, we look at several measured transition events and systematically collect the four-quadrature state vector $\mathbf{Y} = (u_1, v_1, u_2, v_2)$, cf. Appendix D. To visualize the transitions in a two-dimensional space, we use symmetric and antisymmetric coordinates, $v_S = (v_1 + v_2)/\sqrt{2}$, $v_A = (v_1 - v_2)/\sqrt{2}$ (and analogous for u). By plotting several time traces containing multiple transition events in the phase space spanned by v_S and v_A , we obtain the corresponding probability distribution.

Comparing the distributions at four representative frequencies, we find striking differences; see Fig. 2(d). Regions I and II are characterized by two attractors with high probabilities, corresponding to the two phase states of the symmetric mode. By contrast, for $f_d < 2.365$ MHz in regions III and IV, we find the emergence of a substantial probability centered around the phase-state solutions of the antisymmetric modes. This indicates that the appearance of the kink at $f_d = 2.365$ MHz

follows a drastic change in the dominant transition path chosen by the system, and of the underlying quasipotential landscape. Such a deviation in region IV is to be expected as the activation dynamics now involves four different attractors. In other words, the naive model of activation between two states is insufficient in region IV. This is confirmed by a numerical simulation of the noisy time evolution of the EOMs, given in Eq. (2), which is in accord with the experimental results; see bright blue data in Fig. 2(c). Crucially, however, we note that the antisymmetric state is not stable in region III. This observation raises the question: why should the unstable solutions of the system influence the transition paths? In the following, we precisely address this question through an in-depth theoretical study of the transition dynamics.

IV. TRANSITION PATHS

The weak noise-induced switching between stable oscillation states is analogous to noise-activated jumping over a barrier W studied in an equilibrium system [2,67]. The principal difference is that in our driven system, the barrier W between two attractors resides in a quasipotential structure in a rotating frame. We use the Onsager-Machlup formalism to identify the optimal transition paths in phase space between two attractors, whose corresponding action then provides an estimation for the barrier W . We first define the Onsager-Machlup function [52,53]

$$S_{\text{OM}}[\mathbf{Y}] = \int_{t_i}^{t_f} \frac{1}{4} (\dot{\mathbf{Y}} - \mathbf{f}(\mathbf{Y}))^2 dt, \quad (5)$$

where t_i (t_f) is the initial (final) time of the trajectory of a system composed of N resonators, $\mathbf{Y} = (u_1, v_1, \dots, u_N, v_N)^T$, and $\mathbf{f}(\mathbf{Y})$ is the right-hand side of Eq. (2) without noise terms written as a column vector. The switching probability density between two stable states connected by a path $\mathbf{Y}(t)$ is given by $e^{-2S_{\text{OM}}[\mathbf{Y}]/\sigma^2}$. The total switching probability P_{if} from an attractor at \mathbf{Y}_i to one at \mathbf{Y}_f is obtained by integration over all allowed trajectories connecting them. From this probability one can derive the switching rate Γ [52], which in the weak-noise limit scales as $\Gamma \propto \exp(-2W/\sigma^2)$ with barrier W [67].

At low noise, the switching rate Γ is dominated by the path \mathbf{Y}_{min} that minimizes S_{OM} [52]. Hence, we can neglect the integration over all possible paths, and the switching rate is approximately given by

$$\Gamma \approx \Gamma_{\text{min}} \equiv \Gamma_0 e^{-2S_{\text{OM}}[\mathbf{Y}_{\text{min}}]/\sigma^2}, \quad (6)$$

where Γ_0 is an overall prefactor and we identify the effective activation barrier $W_{\text{eff}} = S_{\text{OM}}[\mathbf{Y}_{\text{min}}]$ [52]. If S_{OM} has multiple local minima, one needs to find the contribution from all relevant minimizing paths and weigh their relative contributions.

The landscape of S_{OM} is characterized by a bifurcation diagram of the system equations, which categorize both stable and unstable solutions as effective minima and saddles/maxima, respectively. In Fig. 2(e) we schematically show this bifurcation diagram along the frequency sweep in Fig. 2(a). Various pitchfork bifurcations lead to the emergence of stable and unstable states. Commonly, we are used to dealing with bifurcations in a two-dimensional phase space, where new stable states appear through bifurcations. Moving

to N coupled resonators, we have a $2N$ -dimensional phase space; this larger phase space can exhibit similar bifurcations in each two-dimensional subspace but on top of the “landscape” of the orthogonal phase-space manifold. When these bifurcations occur on top of an unstable (concave) region of the orthogonal manifold, they will not lead to new stable solutions. This is the reason why some of the bifurcations in our case involve purely unstable states. Crucially, the added unstable states do not manifest in the deterministic dynamics of the system and are commonly ignored. We therefore dub the added (proliferating) unstable states “ghost states,” and the bifurcations that spawn them “ghost bifurcations.” For a comprehensive study of the bifurcation map plus the solutions stability as a function of all model parameters, we refer to Refs. [37,48,49].

In our stochastic study, ghost states play an important role. In Fig. 2(e) ghost bifurcations separate regions I and II, as well as II and III. From comparing Figs. 2(c) and 2(e), it becomes clear that the emergence of the ghost states is accompanied by new switching paths, and that these changes impact Γ . Specifically, rather than acting as additional obstacles in the switching paths, the ghost states appear to favor an *increase* in Γ . To elucidate the surprising role of the ghost states, we study the transition paths \mathbf{Y}_{\min} and the corresponding barriers W for the different representative frequencies along the sweep shown in Fig. 2(a). To this end, we need to minimize Eq. (5), which is a complex task. A simple variational scheme with equal time steps gives inconsistent results and more advanced methods such as the sgMAM method [68] are necessary to obtain the correct physical paths (see details in Appendix C).

In Fig. 2(d) we show the calculated switching paths corresponding to the experimental parameters, which are representative for the regions (I–IV). In region I where the symmetric states are the only attractors, we find only one switching path, which passes through the intermediate zero-amplitude state in agreement with our experimentally observed distributions. As expected, this is equivalent to the single KPO case in Fig. 1, confirming that we should expect a monotonic decrease in the transition rate $\Gamma(f_d)$ with decreasing frequency as the attractors move apart [10,18].

In region II we find two additional switching paths that avoid the zero-amplitude state and instead pass through emergent unstable antisymmetric states. This is in line with the experimental data that exhibit a broader distribution around the zero-amplitude state, extending to the two unstable antisymmetric states. Similar paths also arise in regions III and IV, where the unstable states provide transient ledges where the system can hover during switching events; cf. Appendix D. The additional switching paths are visible in the experiment and seem to be the dominant paths in regions III and IV. These alternative switching paths bring forth a complexity to the system dynamics, a feature intrinsically related to the existence of multiple normal modes in KPO networks. In our system, we observe that the minimal path, \mathbf{Y}_{\min} , connects the stable states always via an unstable one; see Fig. 2(d) [69,70], although exceptions have been observed [13,71]. This underscores the importance of investigating stable as well as unstable states of the system in order to understand the stochastic dynamics of Ising networks.

Based on our theoretical analysis of optimal switching paths, we can now obtain W and compare it with that extracted from the experimental data; cf. Appendix C. From this, we identify the dominant transition path; see Fig. 2(d). Within regions I–III, we find good qualitative and approximate quantitative agreement (save for a small overall shift). Interestingly, in region II both paths contribute equally to the activation: one via the antisymmetric ghost states and the other via the origin. However, this effect is not sufficiently strong to be observed in Fig. 2(c). In region III the former overtakes the latter, which manifests as the observed kink in Fig. 2(c). This indicates that the ghost states support the antisymmetric switching, and markedly participate and modify the expected stochastic dynamics of the system. In region IV, both symmetric and antisymmetric phase states are stable. Here the analytical calculation deviates from the experimental and numerical results. This deviation is likely due to the fact that the Onsager-Machlup method considers only switches that connect the two symmetrical states, while the counting algorithm that we used for the experimental and numerical data includes all possible switches between states. The latter includes repeated switches between a symmetric and an antisymmetric state as individual events.

V. DISCUSSION

At a fundamental level, our results demonstrate unambiguously the existence of an unusual type of bifurcation arising from the coupling between the individual resonators. Although these ghost bifurcations remain undetected in a deterministic system characterization [48,49], they impact the interstate switching path, switching rate Γ , and the relative dwell times in the symmetric and antisymmetric states. This inevitably affects the stochastic switching processes in KPO networks and their characterization via stochastic sampling [50]. Our findings are facilitated by the fact that we have a complete knowledge of all fixed points in the system, as facilitated by HarmonicBalance.jl [72]. Thus, we can identify all unstable points in the system, and calculate the various optimal activation paths using the variational sgMAM method [68]. This poses a significant step forward beyond studies that rely on numerical exploration [73,74].

All of our observations have important consequences for logic networks built from KPOs and nonlinear resonators in general, because they impact the solution that a network will choose after a finite transition time. With proper modeling and calibration of the ghost bifurcations, a network can be operated at a position in $f_d - \lambda$ space where the many-body character of the network is preserved and the annealing speed is optimized. It becomes clear from our work that large networks bear very complex switching dynamics and a careful analysis of the bifurcation topology is very important. Future work might find ways to use this complexity in an advantageous manner to perform faster calculations.

VI. SUMMARY AND OUTLOOK

In summary, we experimentally and theoretically investigated the noise-induced dynamics of a system of two coupled nonlinear Kerr parametric oscillators (KPOs). Our study im-

plements the smallest form of a KPO network and tests the switching behavior in so-called Ising machines. We found that ghost bifurcations play an important role, with consequences for the switching dynamics of the system as it progresses towards its most stable configuration. A better understanding of such effects can be very helpful for the calibration of stochastic logic protocols, such as simulated annealing. As coupled networks of parametric resonators are one of the main candidates for future parallel computation architectures, our study provides crucial input for a growing subcommunity working towards classical and quantum analog computation [34,38–40,42,43,75,76]. Furthermore, it provides additional incentives for the fundamental exploration of complex driven-dissipative nonlinear networks in a multitude of fields [36,37].

ACKNOWLEDGMENTS

This work received financial support from the Swiss National Science Foundation through Grants No. (CRSII5_206008/1) and No. (PP00P2_163818) and the Deutsche Forschungsgemeinschaft (DFG) through Projects No. 449653034 and No. SFB1432. We thank Peter Märki, Žiga Nosan, and Christian Marty for technical help.

APPENDIX A: SINGLE KPO

For $J = 0$, each resonator can be driven into parametric resonance when $U_d \geq U_{th}$ [55,77]. We characterize each resonator using frequency sweeps as described in [27,32,51] and obtain the values $Q_1 = 295$, $f_0 = 2.6784$ MHz, $\alpha_1 = -9 \times 10^{17} \text{ V}^{-2} \text{ s}^{-2}$, and $U_{th} = 1.21$ V. Using Eqs. (2), we can describe the steady state of the single KPO by applying the condition ($\dot{u}_1 = \dot{v}_1 = 0$) [27,37,62,72]. This yields a quintic characteristic polynomial with up to three different stable solutions (attractors) in phase space; cf. Fig. 4(b). As a function of f_d , the number of stable solutions changes at specific bifurcation points. In the single KPO, we observe only pitchfork bifurcations, which involve at least one stable solution; cf. Fig. 4(c). In Fig. 4(d) we show the characteristic parametric instability lobe. Region (i) accommodates only one stable state with amplitude 0. Inside the region marked as (ii), the linear resonator becomes unstable, bifurcates, and settles into one of the two steady states that are stabilized by α [55]. These phase states have the same amplitude but are π -shifted in phase; cf. Fig. 4(b). In region (iii), the phase states coexist with the amplitude 0 solution.

In Fig. 1 we inspect the noise-induced switching of a single KPO, whose properties are well known [10,18,23,43]. As expected, we find that Γ decreases monotonically with increasing separation between the phase states, which we control here through f_d [10]. Similar results have been previously measured in other KPO implementations [18].

The monotonic decrease of Γ in Fig. 1(c) is derived using the Onsager-Machlup approach [10]. Specifically, at low noise, the switching rate Γ is dominated by the path \mathbf{Y}_{\min} that minimizes S_{OM} [52]. Repeating this estimation as a function of f_d and calculating Γ_{\min} yields good agreement with the experimentally observed Γ ; cf. Fig. 1(c). Note that the prefactor Γ_0 is not obtained by this method but reused from Ref. [10], leading to a slight overall shift towards larger Γ . The

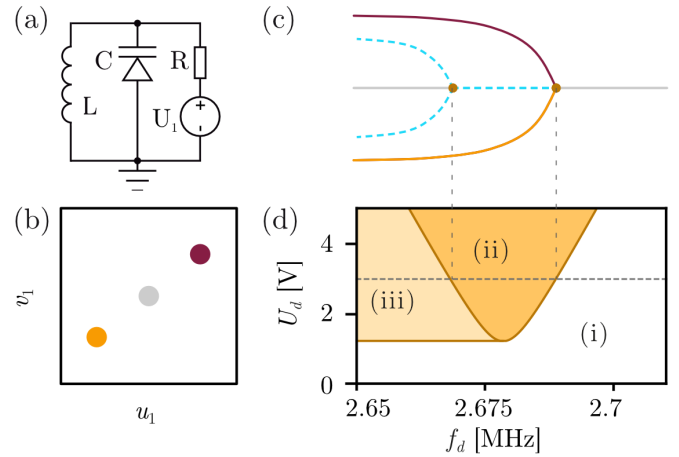


FIG. 4. (a) Schematics of a parametric RLC resonator with resistance R , inductance L , nonlinear capacitance C , and tuning voltage U_1 . (b) Schematic representation of the parametric phase states (wine red, orange), and the zero-amplitude state (gray) in phase space. (c) Schematics of the steady states and bifurcation points as a function of f_d . Solid (dashed) lines correspond to stable (unstable) solutions. (d) Stability phase diagram: (i) White: only the zero-amplitude solution is stable; (ii) orange: only the phase states are stable; (iii) light orange: zero-amplitude and phase states are both stable.

analytical formula derived in Ref. [10] produces a similarly good agreement; cf. Eq. (C1) in Appendix C.

APPENDIX B: FLUCTUATING VERSUS COHERENT SIGNAL AMPLITUDE

To obtain an optimal agreement between the measured switching rates and the theoretical predictions, we consistently found that the noise power spectral density in the model had to be a factor ≈ 4.2 smaller than the value applied in the experiment. This discrepancy is likely due to an additional attenuation of a factor 2 in the path of the fluctuating voltage, for instance, a voltage division at a 50Ω matched input port. The fluctuating signal with power spectral density S_n was provided by two dedicated voltage sources with the same output intensity and added to the coherent signal via the ADD channel of the Zurich Instruments HF2LI lock-in amplifier. The resulting noise process ξ_i acting on our system has a power spectral density $\zeta^2 = C_{in} S_n$, where the coefficient for the signal in-coupling efficiency is $C_{in} = 4.93 \times 10^{-20} \text{ Hz}^4$ for the single-KPO experiment. For the two-KPO experiment, we find best agreement for a slightly lower value for C_{in} , which is probably due to differences in the coil geometry between the devices or between the experimental runs.

APPENDIX C: DETAILS OF THE CALCULATIONS FOR NOISE-INDUCED SWITCHING

1. Determination of the switching rate

The experimental determination of the switching rate Γ in Fig. 2(c) was performed with a lock-in amplifier (Zurich Instruments HF2LI). We used a sampling rate of 450 Hz and a total measurement time of 300 s for $f_d \leq 2.3696$ Hz and

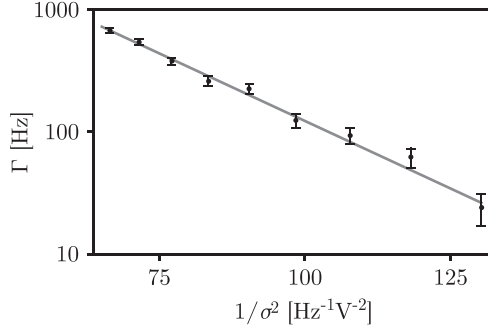


FIG. 5. Switching rate Γ between the symmetric states of the two-KPO system as a function of inverse noise strength, $1/\sigma^2$, obtained from simulation (black) for $U_d = 3.7$ V and $f_d = 2.3725$ MHz. The optimal fit (gray) corresponds to Eq. (6) for the fitting parameters $\Gamma_0 = 2 \times 10^4$ Hz and $W = 0.024$ HzV².

60 s for $f_d > 2.3696$ Hz. Counting of the switching events was done with a numerical algorithm that compared the amplitudes and phases of successive measurement points for an entire time trace measurement. Concretely, the program increased the switching counter by one if the phase difference of two successive points was above a “phase threshold” (130°) while at least one of the points was above an “amplitude threshold” (0.5 mV), or if exactly one out of two successive points was above the amplitude threshold. The same algorithm was used to evaluate the switching rate in numerical simulations that emulated the measurements (including the effective sampling rate). Similar results were obtained by finding the maximal turning point of Allan deviations of the phase [21].

Note that we report on an effective two-state switching rate also in the case that we have transitions four states (region IV in Fig. 2). Here we define an aggregate rate of moving between the two symmetric parametric oscillation states in order to compare with the case where these are the only two attractors. Specifically, let us define the two states as S_1, S_2 .

$$\Gamma = \frac{\left(\gamma \sqrt{\frac{\lambda^2 \omega_0^4}{\gamma^2 \omega^2} - 4} - 4\omega + 4\omega_0 \right) \sqrt{\left| 1 - \frac{\lambda^2 \omega_0^4}{4\gamma^2 \omega^2} \right|} \exp \left(-\frac{\gamma^2 \omega^3 \left(\gamma \sqrt{\frac{\lambda^2 \omega_0^4}{\gamma^2 \omega^2} - 4} - 4\omega + 4\omega_0 \right)^2 \sqrt{\left| 1 - \frac{\lambda^2 \omega_0^4}{4\gamma^2 \omega^2} \right|}}{3\alpha \lambda^2 \sigma^2 \omega_0^4} \right)}{2\sqrt{2}\pi}. \quad (\text{C1})$$

4. Details of the path optimization

The switching rate Γ can be described by $S_{\text{OM}}[\mathbf{Y}_{\text{min}}]$. Obtaining the minimal path \mathbf{Y}_{min} is a complex task for coupled parametric resonators. As a simple variation of a discretized path with equal time steps fails to obtain correct results, we use the sgMAM method [68]. It is an improved path optimization scheme based on scaled time, leading to consistent converged results. We start with a guessed initial path that connects two stable states via an unstable solution. Then we perform numerical minimization of S_{OM} by varying the path in phase space between the chosen end points. For the single KPO, we choose the two phase states as initial and final state; see Fig. 1(b). In the coupled system with $\mathbf{Y} = (u_1, v_1, u_2, v_2)^T$, we choose one of the symmetric states as the initial point and the other one as the final point, and try different unstable states

as intermediate points. We thus obtain the corresponding locally minimizing switching paths \mathbf{Y}_{min} ; see Fig. 2(d).

In the case where these are the only two states, Γ_{S_1, S_2} is readily defined, where we assume that the rates are the same in both direction (valid in our case). In the case of additional stationary states S_j with $j \in \{3, \dots, N\}$, we expect Markovian dynamics with rates between any pair of states Γ_{S_i, S_k} with $i, k \in \{1, \dots, N\}$. We evaluate the aggregate rate $\tilde{\Gamma}_{S_1, S_2}$ by counting how often a state leaves S_1 and ends up in S_2 (and vice versa) within the whole time of the experimental trace; transitions here can go over other stable states along the Markovian chain. We stress once more that this is used only for comparison reasons: to show that there is a region where the two-state scaling break altogether, when more stable states appear. The main result of this work focuses on the region where there are only two-stable states, but a transition in Γ_{S_1, S_2} occurs.

2. Determination of the activation barrier W

We simulate the coupled KPO system at different noise strengths (see Fig. 5), and we verify that our analysis is in the low-noise limit by showing that Eq. (6) is obeyed. The optimal fit (gray) yields $\Gamma_0 = 2 \times 10^4$ Hz and $W = 0.024$ HzV². In this limit, Γ_0 and W are independent of the noise and purely depend on the properties of the deterministic system, and on the switching paths in phase space. This procedure allows us to extract Γ_0 and W for the experimental and the numerical data in Fig. 2(d), as well as calculate Γ at different noise strengths. For the numerical switching rate in Fig. 2(c), we used this scaling law to convert the numerical data, simulated at 1.3 times stronger noise, to the experimentally applied noise.

3. Analytic expression for a single KPO

For a single parametric Kerr oscillator, the switching rate was calculated in [10] and is given by

as intermediate points. We thus obtain the corresponding locally minimizing switching paths \mathbf{Y}_{min} ; see Fig. 2(d).

APPENDIX D: SWITCHING VIA THE ANTISYMMETRIC STATE

In Fig. 6 we show examples of time traces during noise-induced switching between symmetric states. Figure 6(a) corresponds to $f_d = 2.37$ MHz in region I of Fig. 2(c), where switches occur via the unstable zero-amplitude state because both resonators switch synchronously. In Fig. 6(b) we show an example for $f_d = 2.36$ MHz in region IV, where the two resonators switch with a finite delay. In the short time interval between the two switches, the system dwells in the antisymmetric state.

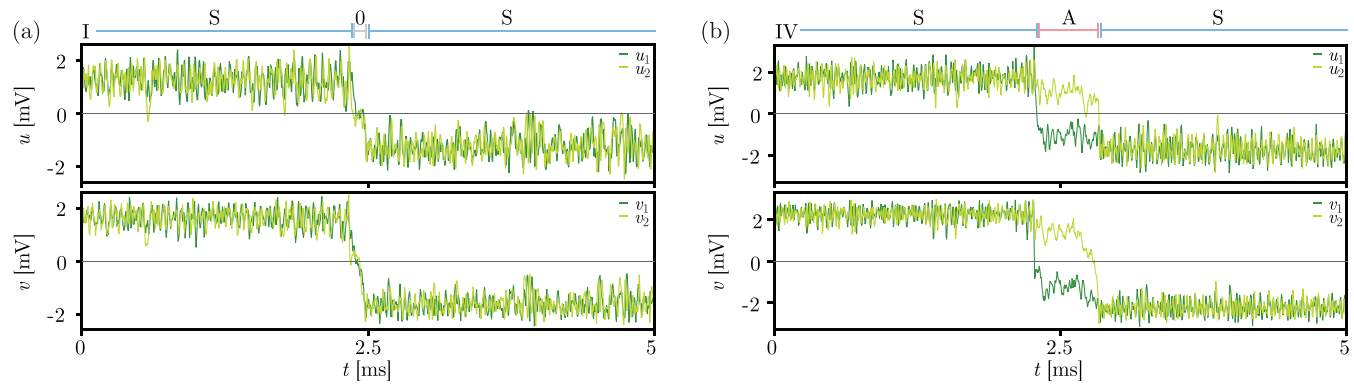


FIG. 6. Examples of switching events in the two-KPO system. (a) For $U_d = 3.7$ V and $f_d = 2.37$ MHz [marked as I in Fig. 2(c)], all four measured coordinates (u_1, v_1, u_2, v_2) switch simultaneously on our sampling timescale. The system switches from one symmetric (S) configuration to the opposite one via the zero-amplitude (0) state. (b) For $U_d = 3.7$ V and $f_d = 2.36$ MHz [marked as IV in Fig. 2(c)], the coordinates (u_1, v_1) switch first, followed by (u_2, v_2) after a delay of roughly 0.5 ms. In the time span between the jumps, the system occupies the antisymmetric (A) state.

- [1] H. Kramers, *Physica* **7**, 284 (1940).
- [2] P. Hänggi, P. Talkner, and M. Borkovec, *Rev. Mod. Phys.* **62**, 251 (1990).
- [3] L. Rondin, J. Gieseler, F. Ricci, R. Quidant, C. Dellago, and L. Novotny, *Nat. Nanotechnol.* **12**, 1130 (2017).
- [4] R. B. Best and G. Hummer, *Phys. Rev. Lett.* **96**, 228104 (2006).
- [5] H. S. Chung, S. Piana-Agostinetti, D. E. Shaw, and W. A. Eaton, *Science* **349**, 1504 (2015).
- [6] P. L. García-Müller, F. Borondo, R. Hernandez, and R. M. Benito, *Phys. Rev. Lett.* **101**, 178302 (2008).
- [7] R. L. Badzey and P. Mohanty, *Nature (London)* **437**, 995 (2005).
- [8] T. A. Fulton and L. N. Dunkleberger, *Phys. Rev. B* **9**, 4760 (1974).
- [9] P. Silvestrini, S. Pagano, R. Cristiano, O. Liengme, and K. E. Gray, *Phys. Rev. Lett.* **60**, 844 (1988).
- [10] M. I. Dykman, C. M. Maloney, V. N. Smelyanskiy, and M. Silverstein, *Phys. Rev. E* **57**, 5202 (1998).
- [11] M. I. Dykman, *Phys. Rev. E* **75**, 011101 (2007).
- [12] Y. Tadokoro, H. Tanaka, and M. Dykman, *Sci. Rep.* **10**, 10413 (2020).
- [13] D. G. Luchinsky, R. S. Maier, R. Mannella, P. V. E. McClintock, and D. L. Stein, *Phys. Rev. Lett.* **82**, 1806 (1999).
- [14] L. J. Lapidus, D. Enzer, and G. Gabrielse, *Phys. Rev. Lett.* **83**, 899 (1999).
- [15] K. Kim, M.-S. Heo, K.-H. Lee, H.-J. Ha, K. Jang, H.-R. Noh, and W. Jhe, *Phys. Rev. A* **72**, 053402 (2005).
- [16] J. S. Aldridge and A. N. Cleland, *Phys. Rev. Lett.* **94**, 156403 (2005).
- [17] H. B. Chan and C. Stambaugh, *Phys. Rev. Lett.* **99**, 060601 (2007).
- [18] H. B. Chan, M. I. Dykman, and C. Stambaugh, *Phys. Rev. Lett.* **100**, 130602 (2008).
- [19] W. J. Venstra, H. J. Westra, and H. S. Van Der Zant, *Nat. Commun.* **4**, 2624 (2013).
- [20] I. Mahboob, M. Mounaix, K. Nishiguchi, A. Fujiwara, and H. Yamaguchi, *Sci. Rep.* **4**, 4448 (2014).
- [21] G. Margiani, S. Guerrero, T. L. Heugel, C. Marty, R. Pachlatko, T. Gisler, G. D. Vukasin, H.-K. Kwon, J. M. Miller, N. E. Bousse *et al.*, *Appl. Phys. Lett.* **121**, 164101 (2022).
- [22] M. Frimmer, T. L. Heugel, i. c. v. Nosan, F. Tebbenjohanns, D. Hälg, A. Akin, C. L. Degen, L. Novotny, R. Chitra, O. Zilberberg, and A. Eichler, *Phys. Rev. Lett.* **123**, 254102 (2019).
- [23] D. Ryvkine and M. I. Dykman, *Phys. Rev. E* **74**, 061118 (2006).
- [24] I. Mahboob and H. Yamaguchi, *Nat. Nanotechnol.* **3**, 275 (2008).
- [25] C. M. Wilson, T. Duty, M. Sandberg, F. Persson, V. Shumeiko, and P. Delsing, *Phys. Rev. Lett.* **105**, 233907 (2010).
- [26] A. Eichler, J. Chaste, J. Moser, and A. Bachtold, *Nano Lett.* **11**, 2699 (2011).
- [27] A. Leuch, L. Papariello, O. Zilberberg, C. L. Degen, R. Chitra, and A. Eichler, *Phys. Rev. Lett.* **117**, 214101 (2016).
- [28] J. Gieseler, B. Deutsch, R. Quidant, and L. Novotny, *Phys. Rev. Lett.* **109**, 103603 (2012).
- [29] Z. Lin, K. Inomata, K. Koshino, W. D. Oliver, Y. Nakamura, J. S. Tsai, and T. Yamamoto, *Nat. Commun.* **5**, 4480 (2014).
- [30] S. Puri, S. Boutin, and A. Blais, *npj Quantum Inf.* **3**, 18 (2017).
- [31] A. Eichler, T. L. Heugel, A. Leuch, C. L. Degen, R. Chitra, and O. Zilberberg, *Appl. Phys. Lett.* **112**, 233105 (2018).
- [32] Z. Nosan, P. Märki, N. Hauff, C. Knaut, and A. Eichler, *Phys. Rev. E* **99**, 062205 (2019).
- [33] A. Grimm, N. E. Frattini, S. Puri, S. O. Mundhada, S. Touzard, M. Mirrahimi, S. M. Girvin, S. Shankar, and M. H. Devoret, *Nature (London)* **584**, 205 (2020).
- [34] S. Puri, A. Grimm, P. Campagne-Ibarcq, A. Eickbusch, K. Noh, G. Roberts, L. Jiang, M. Mirrahimi, M. H. Devoret, and S. M. Girvin, *Phys. Rev. X* **9**, 041009 (2019).
- [35] J. M. Miller, D. D. Shin, H.-K. Kwon, S. W. Shaw, and T. W. Kenny, *Phys. Rev. Appl.* **12**, 044053 (2019).
- [36] M. Dykman, *Fluctuating Nonlinear Oscillators* (Oxford University Press, Oxford, 2012).
- [37] A. Eichler and O. Zilberberg, *Classical and Quantum Parametric Phenomena* (Oxford University Press, Oxford, 2023).

- [38] I. Mahboob, H. Okamoto, and H. Yamaguchi, *Sci. Adv.* **2**, e1600236 (2016).
- [39] T. Inagaki, K. Inaba, R. Hamerly, K. Inoue, Y. Yamamoto, and H. Takesue, *Nat. Photonics* **10**, 415 (2016).
- [40] H. Goto, *Sci. Rep.* **6**, 21686 (2016).
- [41] S. Puri, C. K. Andersen, A. L. Grimsmo, and A. Blais, *Nat. Commun.* **8**, 15785 (2017).
- [42] S. E. Nigg, N. Lörch, and R. P. Tiwari, *Sci. Adv.* **3**, e1602273 (2017).
- [43] M. I. Dykman, C. Bruder, N. Lörch, and Y. Zhang, *Phys. Rev. B* **98**, 195444 (2018).
- [44] Y. Okawachi, M. Yu, J. K. Jang, X. Ji, Y. Zhao, B. Y. Kim, M. Lipson, and A. L. Gaeta, *Nat. Commun.* **11**, 4119 (2020).
- [45] N. Mohseni, P. L. McMahon, and T. Byrnes, *Nat. Rev. Phys.* **4**, 363 (2022).
- [46] M. Calvanese Strinati, L. Bello, E. G. Dalla Torre, and A. Pe'er, *Phys. Rev. Lett.* **126**, 143901 (2021).
- [47] L. Bello, M. Calvanese Strinati, E. G. Dalla Torre, and A. Pe'er, *Phys. Rev. Lett.* **123**, 083901 (2019).
- [48] T. L. Heugel, O. Zilberberg, C. Marty, R. Chitra, and A. Eichler, *Phys. Rev. Res.* **4**, 013149 (2022).
- [49] T. L. Heugel, A. Eichler, R. Chitra, and O. Zilberberg, *SciPost Phys. Core* **6**, 053 (2023).
- [50] G. Margiani, J. del Pino, T. L. Heugel, N. E. Bousse, S. Guerrero, T. W. Kenny, O. Zilberberg, D. Sabonis, and A. Eichler, *Phys. Rev. Res.* **5**, L012029 (2023).
- [51] T. L. Heugel, M. Oscity, A. Eichler, O. Zilberberg, and R. Chitra, *Phys. Rev. Lett.* **123**, 124301 (2019).
- [52] J. Lehmann, P. Reimann, and P. Hänggi, *Phys. Stat. Sol. (b)* **237**, 53 (2003).
- [53] H. S. Wio, *Path Integrals for Stochastic Processes* (World Scientific, 2013).
- [54] N. McLachlan, *Theory and Application of Mathieu Functions* (Clarendon, 1951).
- [55] M. C. Lifshitz, R. Cross, in *Reviews of Nonlinear Dynamics and Complexity*, edited by H. G. Schuster (Wiley-VCH, 2009), pp. 1–52.
- [56] C. Jeffries and K. Wiesenfeld, *Phys. Rev. A* **31**, 1077 (1985).
- [57] A. Neiman, *Phys. Rev. E* **49**, 3484 (1994).
- [58] A. N. Silchenko, S. Beri, D. G. Luchinsky, and P. V. E. McClintock, *Phys. Rev. Lett.* **91**, 174104 (2003).
- [59] A. N. Silchenko, S. Beri, D. G. Luchinsky, and P. V. E. McClintock, *Phys. Rev. E* **71**, 046203 (2005).
- [60] K. Guo, J. Jiang, and Z. Li, *J. Vibration Eng. Tech.* **8**, 599 (2020).
- [61] J. Guckenheimer and P. Holmes, *Nonlinear Oscillations, Dynamical Systems, and Bifurcations of Vector Fields*, Applied Mathematical Sciences (Springer-Verlag, 1990).
- [62] L. Papariello, O. Zilberberg, A. Eichler, and R. Chitra, *Phys. Rev. E* **94**, 022201 (2016).
- [63] K. Seibold, O. Ameye, and O. Zilberberg, [arXiv:2404.09704](https://arxiv.org/abs/2404.09704) (2024).
- [64] R. Z. Khas'minskii, *Theory Probab. Appl.* **11**, 390 (1966).
- [65] J. Roberts and P. Spanos, *Int. J. Non-Linear Mech.* **21**, 111 (1986).
- [66] A. H. Nayfeh and D. T. Mook, *Nonlinear Oscillations*, Physics (Wiley, 2008).
- [67] C. Stambaugh and H. B. Chan, *Phys. Rev. B* **73**, 172302 (2006).
- [68] T. Grafke, T. Schäfer, and E. Vanden-Eijnden, in *Recent Progress and Modern Challenges in Applied Mathematics, Modeling and Computational Science*, edited by R. Melnik, R. Makarov, and J. Belair (Springer, New York, 2017), pp. 17–55.
- [69] R. S. Maier and D. L. Stein, *Phys. Rev. Lett.* **69**, 3691 (1992).
- [70] Y. Tang, R. Yuan, G. Wang, X. Zhu, and P. Ao, *Sci. Rep.* **7**, 15762 (2017).
- [71] H. Feng, K. Zhang, and J. Wang, *Chem. Sci.* **5**, 3761 (2014).
- [72] J. Kořata, J. del Pino, T. L. Heugel, and O. Zilberberg, *SciPost Phys. Codebases* **6** (2022).
- [73] D. Topaj and A. Pikovsky, *Physica D* **170**, 118 (2002).
- [74] S. V. Gonchenko and D. V. Turaev, *Proc. Steklov Inst. Math.* **297**, 116 (2017).
- [75] D. Gottesman, A. Kitaev, and J. Preskill, *Phys. Rev. A* **64**, 012310 (2001).
- [76] M. H. Devoret and R. J. Schoelkopf, *Science* **339**, 1169 (2013).
- [77] L. Landau and E. Lifshitz, *Mechanics* (Butterworth-Heinemann, 1976).